Nuclear Instruments and Methods in Physics Research A 376 (1996) 319-334

NUCLEAR INSTRUMENTS & METHODS IN PHYSICS RESEARCH Section A

ELSEVIER

A study on the properties of lead tungstate crystals

R.Y. Zhu [a,*], D.A. Ma [a], H.B. Newman [a,1] C.L. Woody [b], J.A. Kierstead [b], S.P. Stoll [b], P.W. Levy [b,2]

[a] *California Institute of Technology, Pasadena, CA 91125, USA*
[b] *Brookhaven National Laboratory, Upton, NY 11973, USA*

Received 5 February 1996

Abstract

This report summarizes the results of a study on the properties of five large and five small size lead tungstate ($PbWO_4$) crystals. Data are presented on the longitudinal optical transmittance and light attenuation length, light yield and response uniformity, emission spectra and decay time. The radiation resistance of large crystals and possible curing with optical bleaching are discussed. The result of an in depth materials study, including trace impurities analysis, are also presented. The general conclusion from this investigation is that further research and development is needed to develop fast, radiation-hard $PbWO_4$ crystals for the CMS experiment at the CERN LHC.

1. Introduction

As one of two future experiments at the Large Hadron Collider (LHC) at CERN, the Compact Muon Solenoid (CMS) collaboration decided to construct a precision electromagnetic calorimeter consisting of 110000 lead tungstate ($PbWO_4$) crystals [1]. This decision followed extensive research and development carried out by the physics community pursuing a precision electromagnetic calorimeter aiming at searches for the Higgs boson in the intermediate mass region [2-5]. Several fast scintillating crystals (BaF_2, CeF_3, undoped CsI and $PbWO_4$) were thoroughly investigated [6,7] for this physics motivation. Lead tungstate was chosen by the CMS experiment [1] because of its high density, low cost and fast decay time.

Lead tungstate ($PbWO_4$) crystals are a new type of heavy scintillator which have a high density of 8.3 g cm^{-3}, a short radiation length of 0.89 cm and a small Molière radius of 2.2 cm. They are known to have a complicated emission spectrum and a fast decay time [8-11]. Measurements also indicate that $PbWO_4$ crystals produced by different manufacturers have different emission spectra, and some crystals may have significant slow components [12]. In this report, we present a study on the properties of five large $PbWO_4$ crystals and a small sample grown by the Czochralski method in Bogoroditsk, Russia, along with four small samples grown at Shanghai Institute of Ceramics (SIC) in China. The large Bogoroditsk samples are considered to be full calorimeter size crystals for CMS. Among four SIC small samples, three were grown by the modified Bridgman method, and one by the Czochralski method.

The work presented in this report is part of an ongoing effort aimed at understanding the performance of full size $PbWO_4$ crystals at LHC. To realize the superb energy resolution promised by a $PbWO_4$ crystal calorimeter in the hostile environment at LHC, where a dose of 1 to 10 Mrad of electromagnetic radiation and 10^{13}-10^{14} cm^{-2} of neutron fluence are expected in ten years of operation [1], the stability of the light output of $PbWO_4$ crystals in situ is a crucial issue. The radiation resistance was measured for five full size $PbWO_4$ samples, and it was found that all samples suffer from radiation damage to different degrees. An investigation was also made to study the stoichiometric ratio of Pb: W and impurities in these crystals. Preliminary conclusions have been drawn on possible causes of the slow scintillation and poor radiation resistance in some samples. The results indicate that further research and development is needed to improve the quality of $PbWO_4$ crystals being produced for the CMS collaboration.

Section 2 describes crystal samples and the experimental apparatus used in this investigation. The result of the measurements on crystal properties, such as transmittance, emission spectra, decay times, light yield and light response uniformity are presented in Section 3. Section 4 discusses the results on crystal radiation damage, possible curing through optical bleaching and thermal annealing, phosphorescence

* Corresponding author. Tel. +1 818 3956661, fax +1 818 7953951, e-mail zhu@cithex.caltech.edu.

[1] Supported in part by U.S. Department of Energy Grant No. DE-FG03-92-ER40701.

[2] Supported in part by U.S. Department of Energy Contract No. DE-AC02-CH7600016.

PII S0168-9002(96)00286-0

Table 1
$PbWO_4$ samples investigated in this report

ID	Dimension [cm]	Grower	Growing technology	Remark
728	$1.8^2 \times 21.3 \times 2.1^2$	Bogoroditsk	Czochralski	undoped
767	$1.8^2 \times 21.3 \times 2.1^2$	Bogoroditsk	Czochralski	Nb-doped
768	$1.8^2 \times 21.3 \times 2.1^2$	Bogoroditsk	Czochralski	Nb-doped
1015	$1.8^2 \times 21.3 \times 2.1^2$	Bogoroditsk	Czochralski	Nb-doped
1022	$1.8^2 \times 21.3 \times 2.1^2$	Bogoroditsk	Czochralski	Nb-doped, irradiated
10	$2.5 \times 2.5 \times 2.5$	SIC	modified Bridgman	early sample
17	$2.5 \times 2.5 \times 2.5$	SIC	Czochralski	early sample
34	$2.5 \times 2.5 \times 4.5$	SIC	modified Bridgman	vacuum annealing
41	$2.0 \times 2.1 \times 2.5$	SIC	modified Bridgman	O-rich annealing
478	$0.8 \times 1.0 \times 1.0$	Bogoroditsk	Czochralski	undoped

and thermoluminescence. The structure and impurity analyses are presented in Section 5. Section 6 is a brief summary and discussion. Finally, conclusions are given in Section 7.

2. Experimental

2.1. Samples

A total of five full size and five small $PbWO_4$ samples were studied in this investigation. The full size samples had a tapered shape: 2.1×2.1 cm^2 at the large end, tapering to 1.8×1.8 cm^2 at the small end, and were 21.3 cm long. The small samples were rectangular in shape. Table 1 lists the dimensions, crystal grower and growing technology for all of the samples.

All crystals from Bogoroditsk, Russia, were grown by the Czochralski method. Crystals 478, 728, 767 and 768 were produced in in 1994, and crystals 1015 and 1022 were produced in 1995. Samples 767, 768, 1015 and 1022 were doped with niobium at a level of 10 to 30 ppm by weight. Most samples from the Shanghai Institute of Ceramics (SIC) were grown by using the modified Bridgman method, except sample 17 which was a test sample grown by the Czochralski method. Samples 34 and 41 were specially grown by SIC with different annealing processes. While sample 34 was annealed in a vacuum oven (10^{-4} Torr, 920°, 24 h), sample 41 was annealed in an oxygen-rich atmosphere (920°, 24 h).

All full size Bogoroditsk samples showed a slightly yellowish color caused by absorption bands in the blue region (see Section 3 for the details). There were also macroscopic voids and scattering centers in some crystals which were visible to the naked eye. This seems to be a characteristic feature of crystals produced by the Czochralski method, since crystals grown by the modified Bridgman method appear clear. All surfaces of the samples were initially polished by the manufacturer, and no further surface treatment, other than simple cleaning with alcohol, was carried out before the measurements.

All samples were received without prior exposure to radiation except crystal 1022. Sample 1022 was irradiated by a ^{60}Co source at CERN at a dose rate of 18 krad/h to a total dose of 34 krad.

2.2. Transmittance and light attenuation length

The longitudinal transmittance of each sample was measured using a Hitachi U-3210 UV/visible double beam, double monochromator spectrophotometer equipped with a large sample compartment, including a custom Halon coated integrating sphere. The systematic uncertainty in repeated measurements of transmittance was approximately 0.3%. However, the uncertainty in measurements made by repeatedly placing and removing crystals in the test stand inside the large sample compartment was about 0.5%.

For $PbWO_4$ crystals, additional uncertainties in the transmittance measurements arise because of its birefrigent nature [3], and due to macroscopic defects, such as voids and scattering centers, in the crystal. The uncertainty due to the birefringence was determined to be less than 10% for different azimuthal orientations of the crystal. To avoid this effect, a particular azimuthal orientation was chosen for each sample which gave the maximum longitudinal transmittance. The second uncertainty was less important in our measurements, since the integrating sphere in the large sample compartment collected almost all light passing through the sample. However, crystals which had a large region of inhomogeneity near the center, such as the sample 767, appeared to have a lower transmittance due to scattering. In this case, a careful selection of the light path using a 5 mm aperture was made in order to locate a particular position which gave the maximum longitudinal transmittance.

Assuming two parallel end surfaces and normal incidence light, the longitudinal transmittance can be used to determine the average light attenuation length (LAL) [13]:

$$\mathrm{LAL} = l/\ln \frac{T(1-T_s)^2}{\sqrt{4T_s^4 + T^2(1-T_s^2)^2} - 2T_s^2}, \qquad (1)$$

[3] The C axis of the crystal is at about 19° to the crystal axis, according to the manufacturer.

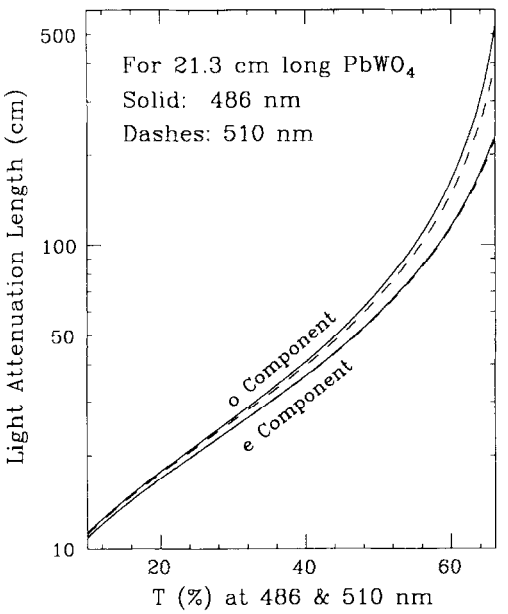

Fig. 1. Light attenuation length as a function of the longitudinal transmittance measured for 21.3 cm $PbWO_4$ crystals. The solid (dashed) curves are for 480 (510) nm. The upper bound corresponds to the refractive index of the ordinary (o) polarization component, while the lower bound corresponds to the extraordinary (e) polarization component [14].

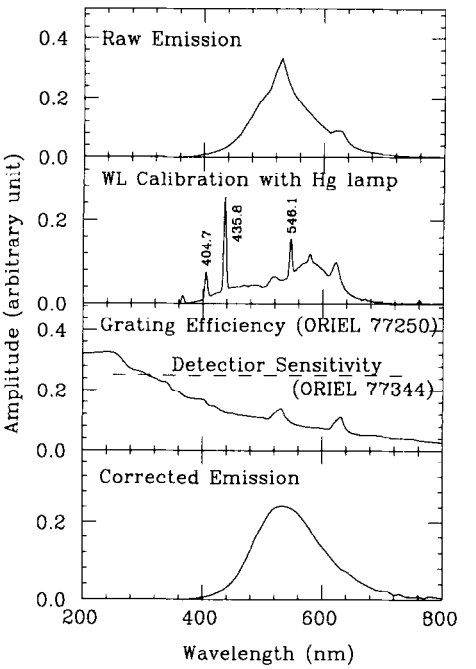

Fig. 2. Corrections to the emission data. From top to bottom: typical uncorrected data of a measured emission spectrum; wavelength calibration with a Hg lamp; measured grating efficiency (solid) and the detector sensitivity (dashed line); the emission spectrum after corrections.

where l is the length of the crystal, T is the measured longitudinal transmittance and T_s is the ideal theoretical transmittance, limited only by losses at two end surfaces of the crystal. Taking into account multiple reflections,

$$T_s = (1-R)^2 + R^2(1-R)^2 + \ldots = (1-R)/(1+R), \quad (2)$$

with

$$R = (n - n_{air})^2/(n + n_{air})^2, \quad (3)$$

where n and n_{air} are the refractive indices of $PbWO_4$ and air, given as a function of wavelength.

Using existing $PbWO_4$ refractive index data [14], Fig. 1 shows the light attenuation length at 486 and 510 nm, as a function of the measured longitudinal transmittance for a 21.3 cm long $PbWO_4$ crystal. While the exact refractive index of $PbWO_4$ at 486 nm was taken from Ref. [14], the refractive index at 510 nm was determined by interpolation. The solid and dashed lines in the figure are for 486 and 510 nm respectively. The upper and lower bounds correspond to the refractive index of the ordinary (o) and extraordinary (e) polarization components [14]. Because of the choice of the azimuthal orientation in the longitudinal transmittance measurement, the e component curves were used to determine the light attenuation length.

2.3. Emission spectra

The scintillation emission spectra were measured in a DC mode using an ORIEL 77250 monochromator and an ORIEL 77344 photomultiplier (PMT) detector with an ORIEL 70100 chopper and lock-in amplifier. The full width at half maximum (FWHM) bandwidth of the spectral power distribution from the monochromator was set to be 10 nm. The accuracy of the wavelength scale of the monochromator was calibrated to within 1 nm using the intrinsic peaks of a Hg lamp. The amplitude of the emission spectrum was corrected for the monochromator grating efficiency and quantum efficiency of the PMT detector. Fig. 2 shows, from top to bottom: typical uncorrected data of a measured emission; the wavelength calibration with a Hg lamp; the measured efficiency of the Oriel 77250 monochromator and the sensitivity of the Oriel 77344 detector (dashed line); the emission spectrum after corrections. The Oriel detector 77344 uses a Hamamatsu R758 PMT with a Cs enhanced GaAs photocathode which has a flat response over the measured wavelength range. As shown in the figure, the two peaks in the raw emission data, caused by the monochromator grating efficiency, were eliminated by these corrections.

Photoluminescence spectra were measured by exciting the samples with UV light and the radioluminescence was measured by excitation with ^{60}Co gamma rays. The photoluminescence was typically measured with an excitation wavelength of 315 nm. Additional measurements showed that the photoluminescence emission spectrum was independent of

excitation wavelength in the range from 250–350 nm. The radioluminescence spectra were typically measured at a dose rate of 36 krad/h. It should be noted that when the emission spectra are measured in a DC mode, phosphorescence (or afterglow) can give rise to a potential source of background. This can be a particular problem for a weak scintillator if the intensity of the phosphorescence is higher than the intrinsic scintillation. However, the phosphorescence was not a problem for the dose rate and total doses used for these measurements.

2.4. Light yield, uniformity and decay times

The scintillation light yield at room temperature (23°) was measured using a Hamamatsu photomultiplier tube (R2059 PMT) which has a bialkali photocathode and quartz window. A collimated γ-ray source, such as ^{137}Cs or ^{60}Co, was used to excite the small end of the crystal. The large end of the crystal was coupled to the PMT with Dow Corning 200 or Viscasil 600M silicone fluid. All other surfaces of the crystal were wrapped with either one layer of Tyvek paper or 5 layers of PTFE teflon film. The photoelectron numbers, corresponding to the γ-ray peak, was determined by the peak ADC channel obtained by a Gaussian fit (not including the Compton edge [15]), times a calibration constant corresponding to the number of photoelectrons per ADC channel. The calibration was obtained by using the single photoelectron peak, again from a Gaussian fit, and was cross-checked with an LED calibration, taking into account the intrinsic width of the single photoelectron spectrum:

$$\text{photoelectron number} = \left[1 + (\sigma_{\text{spe}}/\text{Peak}_{\text{spe}})^2\right] \times (\text{Peak}_{\text{LED}}/\sigma_{\text{LED}})^2, \quad (4)$$

where, Peak and σ are the peak and width from a Gaussian fit, and the subscripts LED and spe refer to the distributions of LED and single photoelectron spectra, respectively.

The light response uniformity was measured by moving a collimated γ-ray source along the crystal at different longitudinal positions and the result was fit to a linear function:

$$\text{LY}/\text{LY}_{\text{mid}} = 1 + \delta(x - x_{\text{mid}})/x_{\text{mid}}, \quad (5)$$

where x is the distance from the small end, LY_{mid} is the fit value of the light yield at the middle of the crystal, x_{mid}, and δ is a measure of the light response uniformity.

The decay constants of the the scintillation light were measured using two independent methods: (1) an integration method and (2) a single photon counting method [17]. In the integration method, the photoelectron yield was measured as a function of integration gate width up to 4 μs and the result was parametrized as

$$\text{LY}/\text{LY}_{\text{tot}} = F + S_1(1 - e^{-t/\tau_1}) + S_2(1 - e^{-t/\tau_2}), \quad (6)$$

where LY_{tot} is the total light yield obtained from the fit, and F, S_1 and S_2 are the normalized amplitudes of a fast component with a decay time constant of less than $\sim$ 10 ns, and two slow components with decay time constants of τ_1 and τ_2 respectively. The normalization was done such that

$$F + S_1 + S_2 \equiv 1. \quad (7)$$

In the single photon counting method, coincident gamma rays from a ^{60}Co source were used to measure the decay time distribution of single photoelectrons produced by the scintillation light in the crystal. The distribution was measured relative to a fast start signal which was provided by a 1 in. diameter BaF_2 crystal coupled to a Hamamatsu R5023 PMT which had rise time of 0.6 ns. The stop signal was provided by a Hamamatsu R2059 PMT which was weakly coupled to the $PbWO_4$ sample in such a way that the average number of photoelectrons per gamma ray interaction was very small ($\ll 1$). The decay times were measured out to 512 ns using a LeCroy 2228A TDC which had a resolution of 250 ps/channel. The resulting time distribution, after the start peak, was parametrized as

$$c_{\text{norm}}\left[S_a/\tau_a e^{-t/\tau_a} + S_b/\tau_b e^{-t/\tau_b} + S_c/\tau_c e^{-t/\tau_c}\right], \quad (8)$$

where S_a, S_b and S_c are the normalized amplitudes of the three decay components with time constants of τ_a, τ_b and τ_c respectively, and c_{norm} is an overall normalization factor.

It should noted that, because of the different time region in these two measurements, the time constants and relative amplitudes determined by the differential and integral methods do not directly correspond with each other. The single photon counting method is best suited to determine the short decay time components (< 30 ns), but can give a poor estimate of the amplitude of the longer decay times if either the average number of photoelectrons is too large, which can result in underestimating the amplitude of the slow components, or because of poor statistics if the average number of photoelectrons is too small. On the other hand, the integration method cannot accurately measure the short decay times because of the need to provide a minimum gate length for the ADC, but gives the best measure of the very long decay time components. The two methods do agree in both the amplitudes and the decay times if two measurements were carried out in an identical time region. Therefore, they complement each other by providing the best accuracy in measuring the two different regions of the spectrum. However, it should be emphasized that in both cases, the fits are simply parameterizations of the data which are not unique, and do not necessarily represent the true decay times of the scintillation components in the crystal.

2.5. Thermoluminescence

The thermoluminescence (TL) spectra were obtained by exposing an approximately 10 mg sample of each crystal to 1 Mrad of ^{60}Co γ-ray irradiation. The TL was measured 10 min after the irradiation from 40 to 400° at a heating rate of 2°/s. All measurements were made at a pressure of 760 mm in a

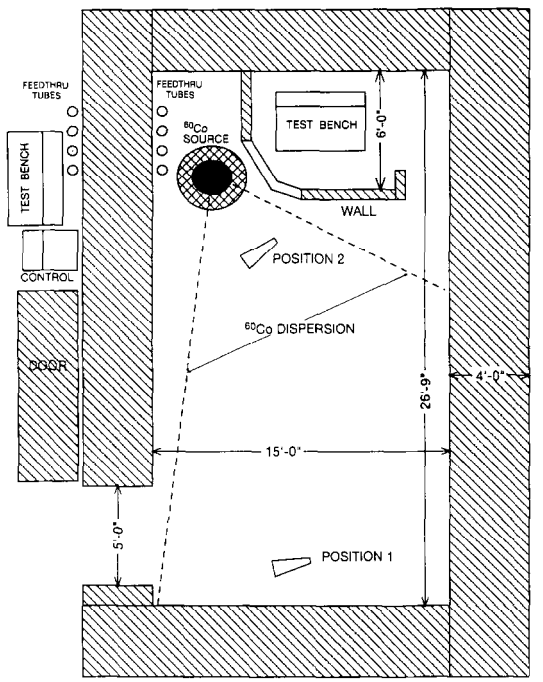

Fig. 3. The layout of the JPL irradiation facility, including the ^{60}Co γ-ray source and location of the $PbWO_4$ samples.

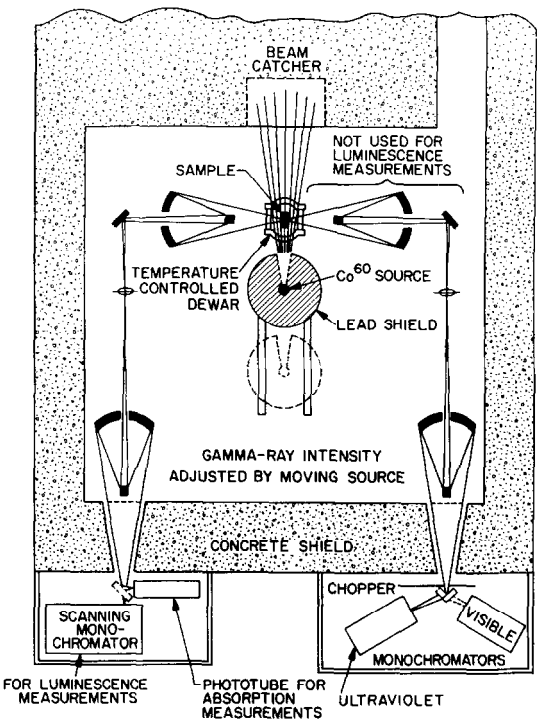

Fig. 4. The layout of the gamma ray irradiation facility at Brookhaven National Laboratory.

helium atmosphere. The total thermoluminescence intensity, integrated over the emission spectrum, was measured using an EMI 9635QB phototube.

2.6. Phosphorescence

The radiation induced phosphorescence was determined by measuring the light output from the crystal shortly after irradiation with no further external excitation applied. Irradiations were carried out at a high dose rate (34 krad/h) for cumulative doses of 0.7 and 1.0 Mrad, and at a low dose rate corresponding to the typical dose rate expected at the LHC (120 rad/h). The light output was measured by placing a Hamamatsu R2059 PMT immediately in front of the crystal and recording the phototube current as a function of time after irradiation. For measurements starting approximately 10 min after irradiation, the phototube current never exceeded approximately 40 μA at a phototube voltage of 2500 V. However, for measurements starting 1–5 s after irradiation, care had to be taken to prevent the phototube from being exposed to excessively high currents during irradiation. Therefore, the high voltage was kept at a low value (1000 V) during irradiation, and was raised to 2000 V within a few seconds after irradiation to measure the current due to the phosphorescence. Under these conditions, the current in the phototube produced by light from the crystal, which was wrapped in white reflecting teflon, never exceeded approximately 20 μA. The current produced in the phototube alone under the same conditions was less than 0.33 μA.

The energy equivalent noise for the phosphorescence was determined from the phototube current and the known gain of the tube. The tube gain was measured using a method similar to that described in Section 2.4. The measured current divided by the gain of the phototube gives the number of photoelectrons produced per second due to the phosphorescence. This can be converted into an energy equivalent noise using a nominal light output for the crystal of 10 photoelectrons per MeV measured by R2059 PMT.

2.7. Gamma ray irradiation

The gamma ray irradiations were carried out at two different irradiation facilities in order to provide a cross check between different measurements. The first, shown in Fig. 3, was at the Jet Propulsion Laboratory (JPL). It was equipped with an approximately 4000 Ci ^{60}Co source during this investigation. Measurement equipment, such as monochromators and phototubes, were placed inside the facility and signals were brought out through feedthrough tubes to additional equipment and computers outside the radiation area. The crystal samples, wrapped only with aluminum foil, were placed at a fixed distance in order to obtain a well defined dose within a fixed time, i.e. 1, 10 and 20 krad in one hour and 70 and 900 krad in 18 h, as illustrated in the figure. The dose rate was calibrated using a MDH 2025 Monitor with air-equivalent ion chambers which had an accuracy of 5%.

The second irradiation facility was the Gamma Ray Irradiation Facility (GRIF) at Brookhaven National Lab. This

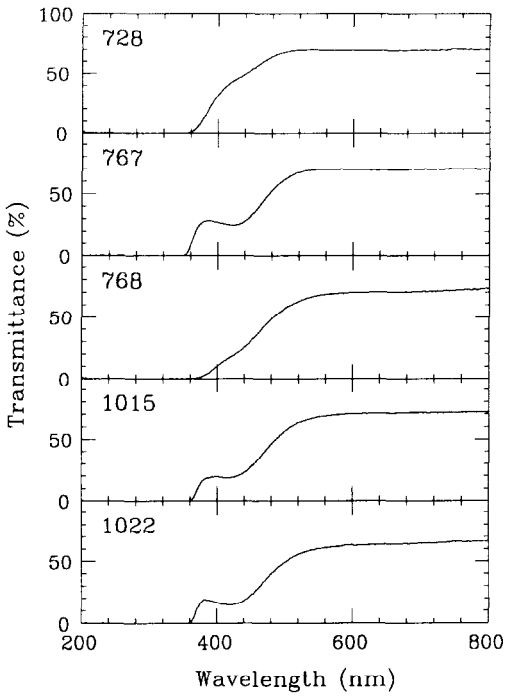

Fig. 5. Longitudinal transmittance of five 21.3 cm $PbWO_4$ samples as a function of the wavelength.

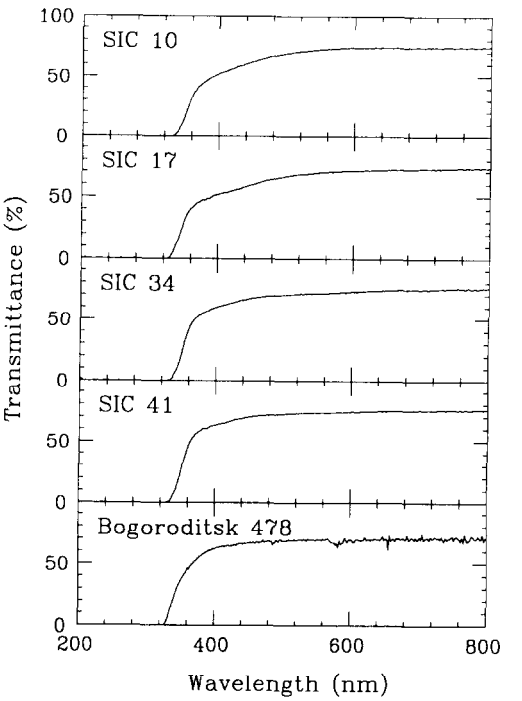

Fig. 6. Transmittance of five small size $PbWO_4$ samples as a function of wavelength. The light path is along the longest edge of the sample.

facility, as shown in Fig. 4, consists of a 20000 Ci ^{60}Co source contained within a large UV-vis spectrophotometer which can be used to measure transmission and emission spectra before, *during*, and after irradiation [16]. It was also used as a radiation source for the phosphorescence decay time and thermoluminescence measurements. The dose rate was calibrated using a Victoreen Model 525 electrometer/dosimeter which has an instrumental accuracy of 1%, and agreed with the dose rate measured using LiF dosimetry to better than 5%. Samples irradiated here were prepared and irradiated under the same conditions as at JPL.

All procedures and measurements on the samples after irradiation were carried out in the dark or under red light in order to minimize any effects of optical bleaching. For the measurements made at GRIF, the samples were measured within 30 min after irradiation, while at JPL, the measurements were made within two hours after irradiation. For the light yield measurement, the samples were wrapped with either one layer of the Tyvek paper (140 μm), or five layers of PTFE film, consistent with the wrapping used before irradiation.

3. Results of measurements on optical properties

3.1. Transmittance and light attenuation length

Figs. 5 and 6 show spectra of the longitudinal transmittance of each sample measured before irradiation. The changes in transmittance after irradiation are discussed in Section 4. There were no significant absorption bands at wavelengths longer than 500 nm. For most crystals, the transmittance at 800 nm was $\geq$ 70%, i.e. close to the theoretical limit, indicating a very long light attenuation length at this wavelength. The only exception was crystal 1022, which was irradiated prior to these measurements, and has a transmittance below 70% at 800 nm. However, below 500 nm, the transmittance shows significant absorption. This absorption causes the yellowish color described in Section 2.1. The exact origin of this absorption is not yet understood. There are also significant differences in the transmittance spectra in this wavelength region. While samples 767, 1015 and 1022 have a knee below 400 nm, samples 728 and 768 show none, and the latter have very poor transmittance at 370 nm. In addition, sample 767 has a higher transmittance at 370 nm than samples 1015 and 1022. The knee in the longitudinal transmittance at 370 nm seems to be correlated with the radiation hardness of the crystal, as discussed in Section 6.

All small samples show significantly better transmittance below 500 nm. It also is clear from Fig. 6 that SIC samples 34 and 41 have a very sharp rising edge at 340 nm, even though sample 34 has a longer path length than the other samples.

Table 2 lists the transmittance and the light attenuation length (LAL) at 486 and 510 nm for the five full size samples calculated according to Eq. (1). Most crystals have a light attenuation length longer than 100 (50) cm at 510 (486) nm, except crystal 1022, which has a significantly

Table 2
Light attenuation length of $PbWO_4$ samples

	ID				
	728	767	768	1015	1022
Transmittance [%] @486 nm	64.9	55.2	51.2	49.3	46.7
LAL [cm] @486 nm	156	73	58	52	47
Transmittance [%] @510 nm	69.0	64.6	60.0	60.2	56.8
LAL [cm] @510 nm	259	152	98	100	79

shorter light attenuation length. The lower initial transmittance and light attenuation length of sample 1022 can be attributed to the fact that it was irradiated before it was received, as discussed in Section 2.1.

3.2. Emission

Figs. 7 and 8 show the photoluminescence (solid curves) and radioluminescence (dashed curves) emission spectra. These spectra were corrected for the grating efficiency and detector sensitivity, as discussed in Section 2.3. The overall shape of most of the emission spectra is similar, and is close to a Gaussian distribution with a FWHM of about 120 nm. However, sample 34 has a broader emission, and sample 478 has a narrower emission, as compared to the other samples. For most samples, the radioluminescence seems to have a 20 to 30 nm blue shift, as compared to the photoluminescence.

Fig. 9 shows the $PbWO_4$ emission spectrum together with the quantum efficiencies of various photodetectors: a Hamamatsu R2059 PMT, a Hamamatsu 2 cm^2 photodiode with silicon oxide (S2744-03) and silicon nitrite (S2744-08) resin, and an EG&G avalanche photodiode (APD). The emission weighted quantum efficiencies of these devices are 10.4%, 64%, 77% and 81% for the R2059, S2744-03, S2744-08 and EG&G APD, respectively.

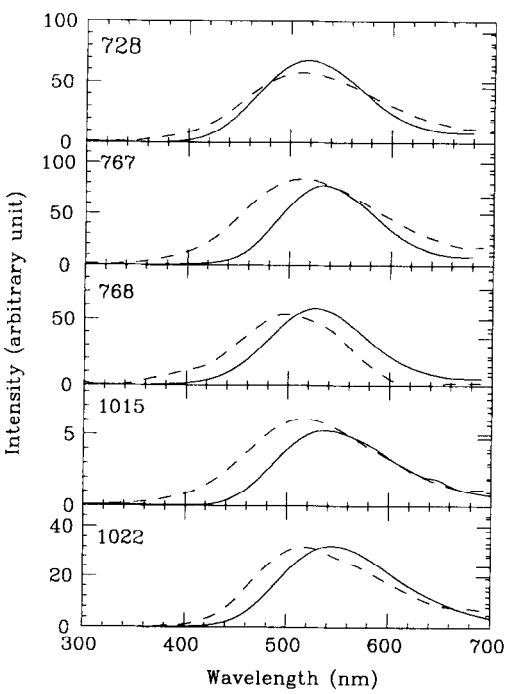

Fig. 7. Photo- (solid) and radio- (dashes) luminescence of five full size $PbWO_4$ samples as a function of the wavelength.

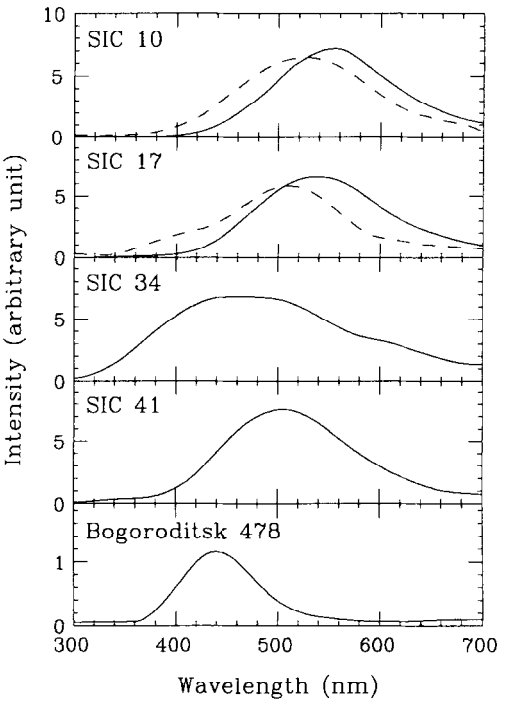

Fig. 8. Photo- (solid) and radio- (dashes) luminescence of five small $PbWO_4$ samples as a function of the wavelength.

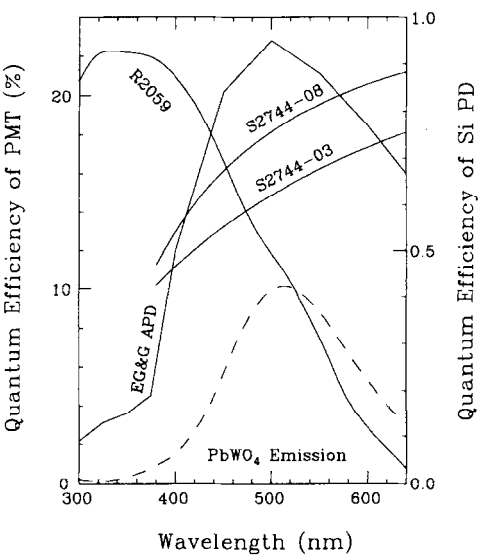

Fig. 9. $PbWO_4$ emission and quantum efficiency of various photodetectors.

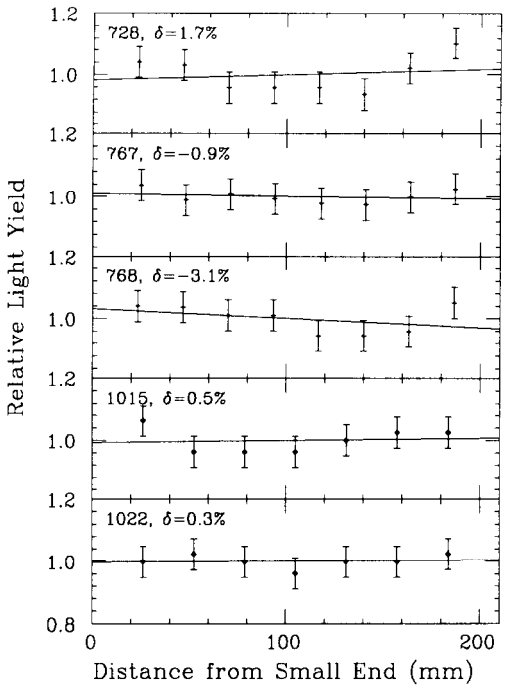

Fig. 10. The light response uniformity of five full size $PbWO_4$ samples is shown as a function of the distance to the small end of the crystal.

3.3. Light yield, decay time and response uniformity

Fig. 10 shows the light response uniformity measured before irradiation for the five full size samples. Samples 728, 767 and 768 were wrapped with 5 layers of PTFE teflon film, while samples 1015 and 1022 were wrapped with one layer of Tyvek paper. The results were fit to Eq. (5) and show that the uniformity is generally better than a few percent for both types of wrappings. This good uniformity can be attributed to the fact that the light attenuation length at the emission peak (500 nm) is long enough to provide adequate compensation between the attenuation and focusing effect caused by the tapered shape [6].

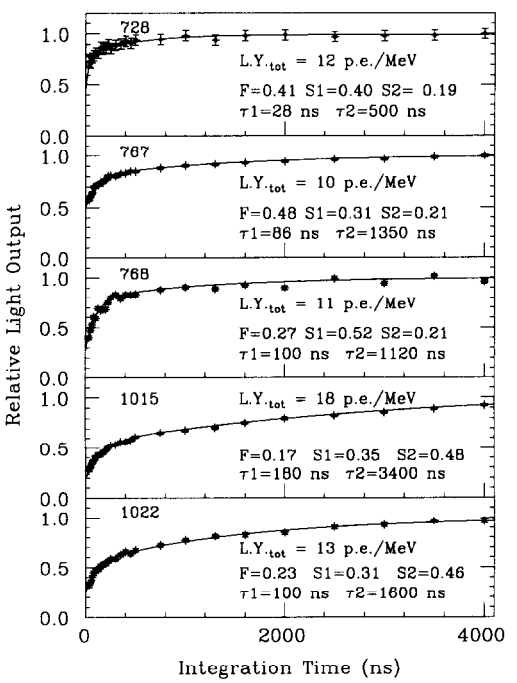

Fig. 11. The light yield of five full size $PbWO_4$ samples is shown as a function of integration time.

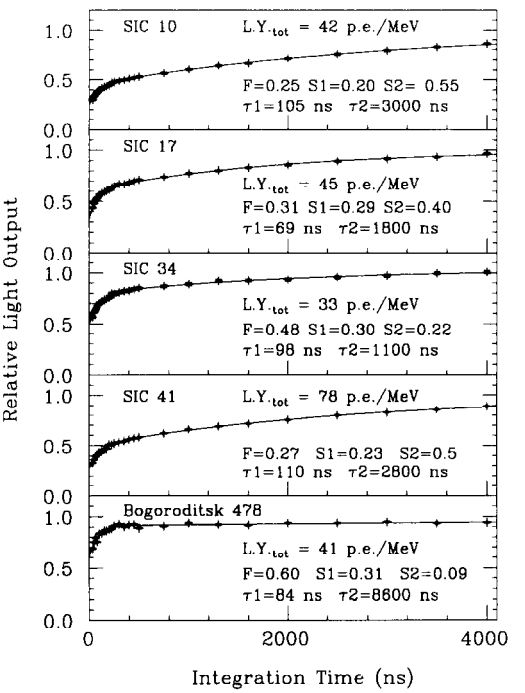

Fig. 12. The light yield of five small size $PbWO_4$ samples as a function of integration time.

Figs. 11 and 12 show the data for the light yield and decay time measurements determined using the integral method. The light yield as a function of integration time was fit to the parameterization given in Eq. (6) and the results are shown in the figures. The fits show that, over this time interval, the decay times can be parameterized as a sum of (1) a very fast

Table 3
Light yield (p.e./MeV) of $PbWO_4$ samples

ID	LY_{tot}	LY_{50ns}	LY_{100ns}
728	12	9.0	9.8
767	10	6.1	7.0
768	11	5.3	6.7
1015	18	5.2	6.5
1022	13	4.7	5.9
10	42	14	16
17	45	21	25
34	33	20	23
41	78	28	33
478	41	30	34

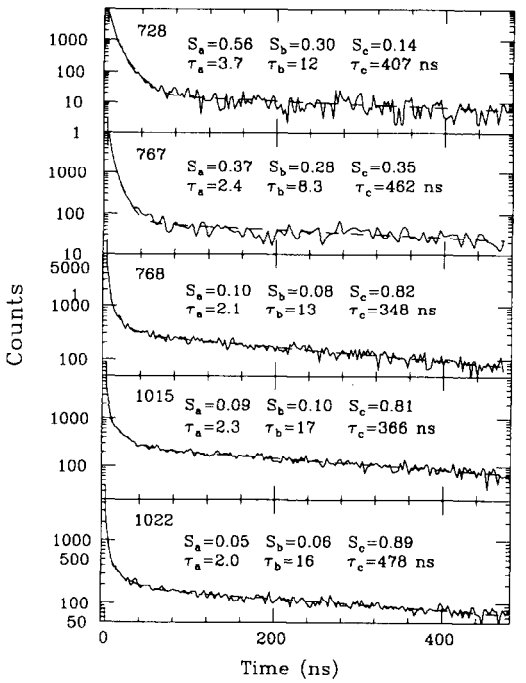

Fig. 13. Decay time spectra measured with the single photon counting method for five full size samples.

component with a decay time of less than 10 ns, (2) a slow component with a decay time of 20 to 200 ns and (3) a very slow component with a decay time of 500 ns to several μs.

Table 3 lists the total light yield (LY_{tot} defined in Eq. (6)) and the light yield integrated in 50 (LY_{50ns}) and 100 (LY_{100ns}) ns gates, in units of the number of photoelectrons per MeV of energy deposit (p.e./MeV). For full size samples, the fraction in the very slow component varies from 19% for undoped sample 728 to 48% for the more recently grown Nb-doped sample 1015. All Nb-doped samples have very similar light yields measured in the short gates (50 and 100 ns).

The light yield and decay time for the small samples vary considerably. All SIC samples have a significant very slow component (22 to 55%) in the total light output. However, sample 34, which was prepared with vacuum annealing and has a broad emission spectrum, has much smaller slow components, as compared to sample 41, which was prepared by annealing in an oxygen-rich atmosphere and has an emission in the green region. On the other hand, the Bogoroditsk sample 478, which has a narrow blue emission, has the largest fast component (60%) and the smallest very slow component (9%). SIC sample 41 has the highest overall light yield (78 p.e./MeV), while its light yield measured in the short gates (50 and 100 ns) is similar to that of sample 478. Note the high photoelectron/MeV yield from samples 34 and 478 is partly due to the fact that their emission peaked at the region where R2059 PMT provides a higher quantum efficiency.

Fig. 13 shows the decay times measured using the single photon counting technique for the five full size Bogoroditsk samples. The short decay times are characterized by two fast components, one with a time constant on the order of 2 ns, and another in the range from 8 to 17 ns. These components are consistent with the short to medium decay components found using the integral method. The single long component fit over this time interval (500 ns) is in the range from 350 to 500 ns, which is again consistent with the values found using the integral method. It is also clear that crystal 728, which is undoped, has the smallest slow components given by either method.

It should again be noted that in both the integral and single photon counting methods, the fitted parameters are not unique, nor is the parameterization. Fitting to two, three or even four exponential terms can all give good fits with very different values for the parameters. In addition, the fit range can greatly affect the parameters. Nevertheless, the short decay times are best measured by the single photon counting method, and the long decay times by the integral method. However, it should again be emphasized that these are simply parameterizations to the data and do not necessarily represent the actual scintillation decay times of the crystal.

4. Results on radiation damage

There are a number of possible effects of radiation damage in a scintillating crystal. These include radiation induced absorption (i.e. color center formation), a possible effect on the scintillation mechanism, and radiation induced phosphorescence. Damage to the scintillation mechanism could affect the light yield, while color center formation would affect the light attenuation length of the crystal, and thus the light output observed by the photodetector. Radiation induced phosphorescence could cause additional noise in the readout device.

Only the full size samples were studied for radiation damage, since the results for a small sample would not necessarily be representative of the performance of a large crystal in situ at LHC [6]. Only damage by electromagnetic energy deposition using ^{60}Co γ-rays was measured in this investigation. Additional studies on radiation damage caused by neutrons and hadrons will be carried out in future.

4.1. Emission damage

Fig. 14 shows the radioluminescence of samples 767 and 1015 measured before (solid) and after (dashes) 1 Mrad of ^{60}Co γ-ray irradiation at a dose rate of 36 krad/h. The spectra in the figure are arbitrarily normalized to facilitate a comparison of their shape. It is clear that there is no significant change in the shape of the emission spectra before and after irradiation. This indicates that the scintillation mechanism which gives rise to this spectral shape is not damaged by the radiation. However, it is more difficult to make any quantitative statement on the possible change in the absolute

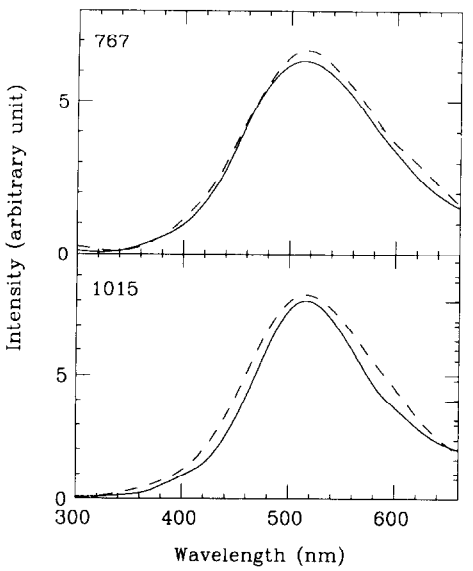

Fig. 14. Photoluminescence spectra measured before (solid) and after (dashes) 1 Mrad irradiation are shown as a function of wavelength for samples 767 and 1015.

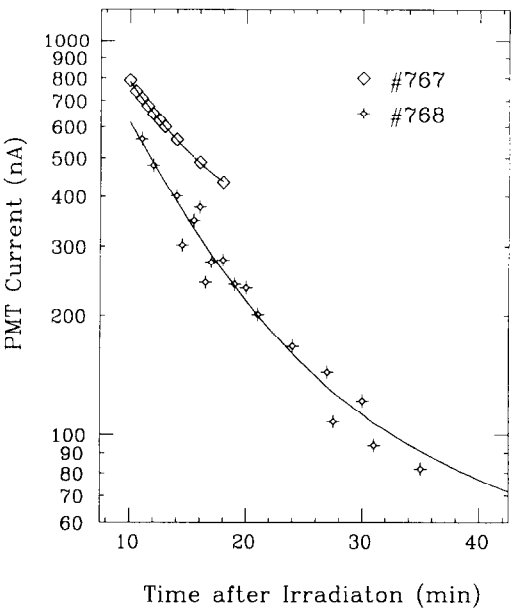

Fig. 15. The phosphorescence intensity is shown as a function of time for samples 767 and 768 after γ-ray doses of 700 and 1000 krad, respectively, at a dose rate of 3.4×10^4 rad/h. The decay times can be fit to two time constants: one, measured in both samples, of ~ 6–7 min, and another, measured in sample 768, of ~ 42 min.

amplitude of the emission spectra before and after irradiation, since absolute intensity is affected by the systematic errors of the measurements and the radiation induced absorption in the samples.

4.2. Radiation induced phosphorescence

Fig. 15 shows the radiation induced phosphorescence in samples 767 and 768 as a function of time starting approximately 10 min after γ-ray doses of 700 and 1000 krad, respectively, which were accumulated at a dose rate of 3.4×10^4 rad/h. The apparent lower phosphorescence intensity in 768 was at least partly due to its higher induced absorption. The decay time of the phosphorescence intensity can be fit to two time constants: one with a decay time of about 6 to 7 min, and another with a longer decay time of about 42 min. For very short times after irradiation (starting within a few seconds), the phosphorescence intensity was observed to be considerably higher than after the first 10 min, but decayed away by several orders of magnitude within approximately one minute.

In order to simulate conditions more representative of the LHC, a piece of of crystal 767 (corresponding to approximately half the original volume) was irradiated at a dose rate of 120 rad/h. At this lower dose rate, the phosphorescence measured immediately after irradiation reached a maximum after an exposure of only 10 min, which was considerably less than after the high dose rate exposure, and was essentially independent of total dose for longer exposures. This implies that, under low dose rate conditions, the rate at which conduction electrons are captured in traps reaches a value which is approximately equal to the rate at which electrons are thermally released from these traps and subsequently produce luminescence. The intensity of the phosphorescence, in terms of energy equivalent noise, was determined for times between 1–5 s after irradiation according to the procedure described in Section 2.6. The value obtained for a full sized crystal under low dose rate conditions was 0.4 MeV within a 40 ns integration time, which is well below the acceptable noise limit for a precision electromagnetic calorimeter at the LHC. However, it should be noted that the magnitude of the phosphorescence can vary significantly from crystal to crystal, and therefore this should be checked again for the actual crystals which are to be used in the calorimeter.

4.3. Radiation induced absorption and light output loss

Fig. 16 shows the longitudinal transmittance as a function of wavelength measured before and after a series of irradiations from a few krad to 0.8 to 1.0 Mrad for the five full size samples. The top curve in each plot represents the transmittance before irradiation, as shown in Fig. 5, and the bottom curve represents the highest dose, as indicated in the figure. Note that, for samples 767, 1015 and 1022, the middle curves are difficult to distinguish from the bottom curve, indicating a very small change in the longitudinal transmittance, as well as saturation after a dose of a few krad.

It is clear that these five samples can be divided into two groups: (1) samples 728 and 768 which show significant radiation induced absorption, (2) samples 767, 1015 and 1022 which show much less damage. The shape of the radiation induced absorption is also different between these

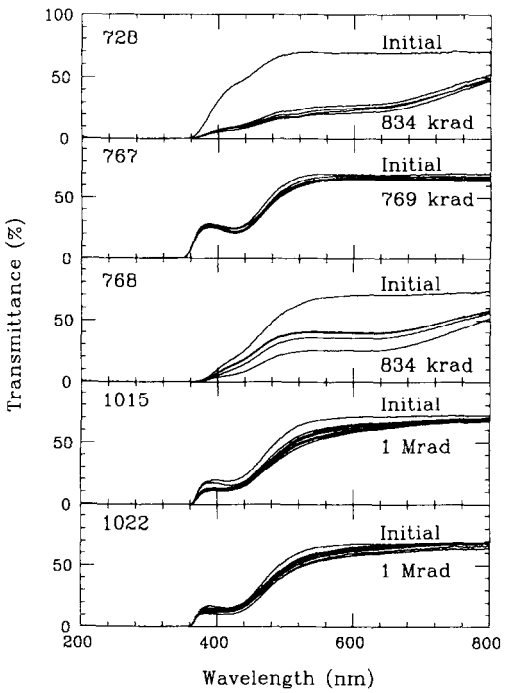

Fig. 16. Transmittance before and after irradiation as a function of wavelength with cumulative doses of (1) 2.4, 11, 20 and 834 krad for 728 and 768; (2) 1.0, 2.6, 7.6, 18.2, 28.2, 119 and 770 krad for 767; and (3) 2, 4, 5, 15, 35, 105 and 1000 krad for 1015 and 1022.

two groups. Significant absorption was found at wavelengths longer than 600 nm for samples 728 and 768, while it is much less for 767, 1015 and 1022.

The longitudinal transmittance measurements can be used to determine the light attenuation length according to Eq. (1). Fig. 17 shows the light attenuation length at 486 and 510 nm as a function of accumulated dose. As discussed in Section 3.2, the emission of these crystals peaks at around 510 nm.

The light attenuation length of crystal 728 and 768 degraded immediately after the first dose of 2.4 krad to 20 and 30 cm, respectively, and the degradation continued to produce an attenuation length of less than 20 cm after the highest dose for 768. On the other hand, the light attenuation lengths of 1015 and 1022 were roughly stable at 40 to 60 cm after a few krad up to a dose of 1 Mrad. For sample 767, the light attenuation length decreased to the range of 50 to 80 cm. It can be noted that the samples with better radiation resistance, namely 767, 1015 and 1022, initially showed higher transmittance at 370 nm than samples 728 and 768, which showed poorer radiation resistance.

The light output, normalized to the unirradiated value, is shown as a function of cumulative dose for crystals 767, 1015 and 1022 in Fig. 18. It follows a similar pattern to the light attenuation length. The degradation in light output after irradiation for samples 728 and 768 is not plotted because it was difficult to accurately measure the light output of these two crystals after the irradiation due to the large radiation

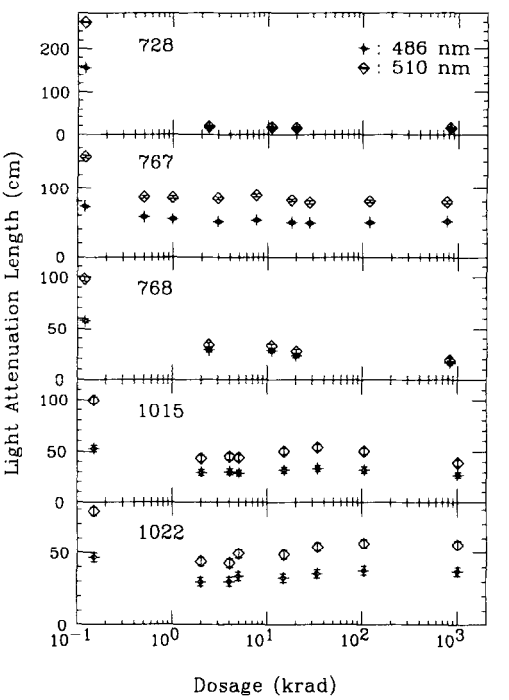

Fig. 17. The light attenuation length at 486 and 510 nm as a function of cumulative dose for crystals 728, 767, 768, 1015 and 1022. The actual doses are the same as in Fig. 16.

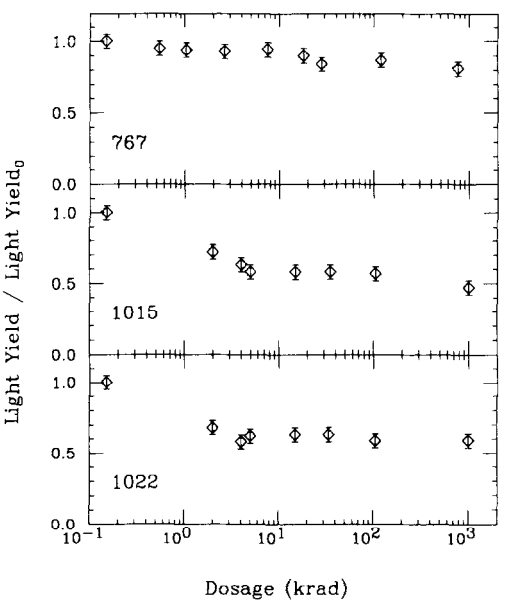

Fig. 18. The light output normalized to the value before irradiation as a function of cumulative dose for crystals 767, 1015 and 1022. The actual doses are the same as in Fig. 16.

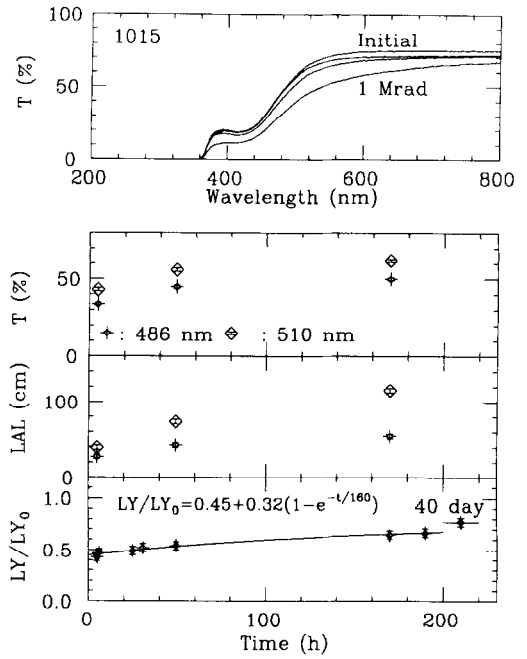

Fig. 19. Recovery from radiation at room temperature for sample 1015. The curves are, from top to bottom: before irradiation, 170, 49 and 4.8 h after 1 Mrad irradiation. Bottom figures show the recovery in transmittance, light attenuation length and light yield with time. The rightmost data point was taken after 40 days after 1 Mrad irradiation.

induced absorption and interference from the phosphorescence. After the first 2 krad, the light output of 1015 and 1022 were reduced to 70% of their initial values, and then leveled off at about 50 to 60% up to the full dose of 1 Mrad. The degradation in the light output of sample 767 was much smaller, dropping to 80% of its initial value.

In summary, the radiation induced absorption causes significant degradation in the observed light output of the samples measured. The better samples (767, 1015 and 1022) showed saturation in their damage, which indicates the origin is most likely due to trace element impurities or defects in the crystal. The best sample (767) shows much less degradation in light attenuation length and light output.

4.4. Spontaneous recovery at room temperature

Lead tungstate appears to show spontaneous recovery from radiation damage at room temperature. The top plot of Fig. 19 shows the recovery in the transmittance as a function of wavelength for sample 1015 after a dose of 1 Mrad. The bottom plot of Fig. 19 shows the transmittance, light attenuation length at 486 and 510 nm, and normalized light yield as a function of time after a 1 Mrad irradiation. The solid line in the light yield plot is a fit to an exponential recovery time with a time constant of 160 h, as shown in the figure. Note that the rightmost data point was taken after 40 days after 1 Mrad irradiation, as marked in the figure, and was included in the fit, which is shown as the horizontal bar across the data point. Similar recovery in the transmittance, light attenuation length, and light output was also observed for samples 728, 767, 768 and 1022.

Table 4
Optical bleaching and thermal annealing for sample 768

Operation	Duration [h]	@486 nm		@510 nm	
		T [%]	LAL [cm]	T [%]	LAL [cm]
Initial	–	51.2	58	60.0	98
After 840 krad	–	21.0	17	24.0	19
700 nm bleaching	6	27.5	21	32.4	26
700 nm bleaching	12	32.7	26	38.5	33
600 nm bleaching	6	45.6	44	54.1	67
600 nm bleaching	12	49.0	52	58.1	86
500 nm bleaching	6	44.6	42	53.6	65
Recovery @ RT	24	45.6	44	54.5	68
640 nm bleaching	6	49.2	52	59.1	92
200° thermal annealing	2	52.9	63	62.5	120
660 nm bleaching	6	51.5	59	61.5	110

4.5. Optical bleaching and thermal annealing

The radiation induced absorption can also be reduced by either optical bleaching or thermal annealing. It is known that the color centers in crystals can often be entirely eliminated by heating the crystal to a high temperature, a process know as thermal annealing [6]. By injecting light into the crystal, the color centers can also be eliminated by the process of color center annihilation [20], and the effectiveness of this optical bleaching is known to be wavelength dependent.

Optical bleaching and thermal annealing were also found to be effective for $PbWO_4$. A series of measurements were carried out for samples 728, 768, 1015 and 1022. After a dose of 840 krad, bleaching light was applied at various wavelengths, and then finally the crystal was placed in an oven at 200° for two hours. Table 4 lists the measured transmittance and light attenuation length at 486 and 510 nm for sample 768. It is interesting to note while light with a wavelength longer than 600 nm is indeed useful to bleach the sample, light at a wavelength of 500 nm actually causes the absorption in this wavelength range to increase, similar to the well known UV damage of BGO crystals. Fig. 20 shows the transmittance as a function of wavelength for sample 768. Measurements with sample 728, 1015 and 1022 showed a similar result, i.e. light at wavelengths of 600 nm or longer was effective for optical bleaching.

4.6. Thermoluminescence

Fig. 21 shows thermoluminescence glow curves for samples 767 and 768. The result shows that sample 768 has a much stronger TL response than 767, indicating a higher concentration of trapped charge and luminescent recombination centers in sample 768. This observation is consistent

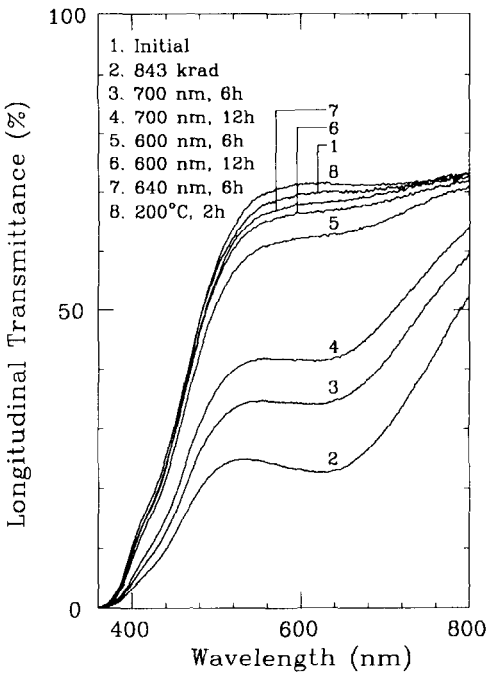

Fig. 20. The transmittance of sample 768 as a function of wavelength. The curves correspond to: 1 – initial; 2 – 843 krad; 3 – 6 h optical bleaching at 700 nm; 4 – 12 additional hours at 700 nm; 5 – 6 h at 600 nm; 6 – 12 additional hours at 600 nm; 7 – 6 h at 640 nm; 8 – 2 h thermal annealing at 200°C.

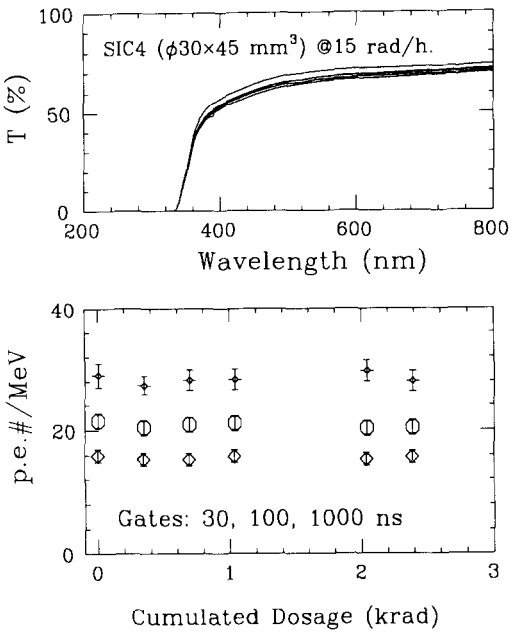

Fig. 22. Top: the longitudinal transmittance as a function of wavelength before and after irradiation for sample 4 from SIC (4.5 cm long). Bottom: the light yield integrated in 30, 100 and 1000 ns is shown as a function of cumulative dose.

with the observation that sample 768 is less radiation hard than sample 767. However, the TL signal in both samples is rather weak, and is roughly 3 to 4 orders of magnitude less intense than a typical BaF_2 sample. The longer lived phosphorescence observed in both crystals most likely arises from the two lowest temperature glow peaks. While sample 768 has at least three peaks at 110, 150 and 245°, sample 767 has only two peaks at 90 and 140°. These data indicate that the lowest temperature trap has a depth of about 0.7 eV for both crystals, but to estimate the trap depth for the other peaks would require additional measurements.

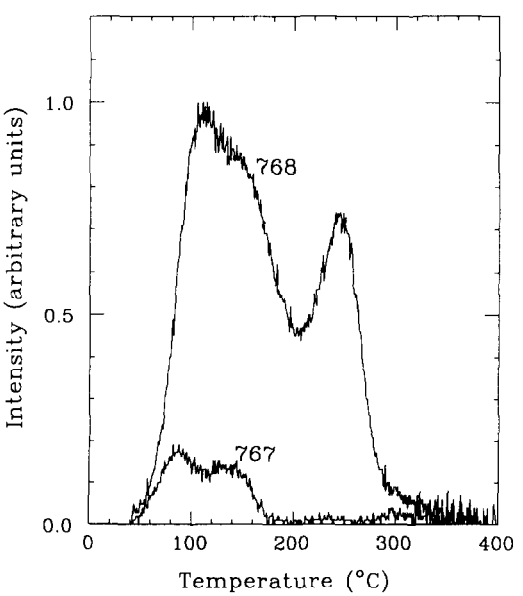

Fig. 21. Thermoluminescence glow curves for samples 767 and 768.

4.7. Intrinsic radiation resistance

Finally, there is evidence that $PbWO_4$ crystals can be made radiation hard, or that $PbWO_4$ crystals are intrinsically radiation hard. The sample 767 is one example which showed only a 20% degradation in light yield. Fig. 22 shows the transmittance as a function of wavelength (top) and the light output as a function of integrated dose for a diameter 3×4.5 cm sample (SIC4, which was not included in the original group), for a low dose test. This particular sample was grown by the Czochralski method using raw materials with adequate purity (99.9 to 99.99%). The radiation damage in both the absorption and the light output are negligible. Although this is a small crystal, the performance of this particular sample provides evidence that the radiation damage problem of $PbWO_4$ crystals can be resolved through a systematic research and development program, as is currently being pursued by the CMS collaboration.

Table 5
GDMS analysis result on trace element concentrations (ppm)

	Sample									
	Na	Al	Si	K	Ca	Nb	Mo	Ba	TM	RE
728	3.2	< 2.6	< 0.7	< 0.3	5.5	3.9	8.9	0.82	< 1.0	0.28
767	9.3	< 0.7	42	0.50	0.97	7.8	16	0.40	< 0.4	0.11
768	1.8	< 0.7	51	0.52	2.4	6.9	15	0.51	< 0.4	0.12
1015	2.8	3.0	1.5	1.9	5.5	7.9	120	0.16	1.8	0.11
1022	3.1	3.0	1.8	1.7	7.7	10	100	0.16	1.6	0.10
34	3.0	2.0	1.3	3.3	2.7	< 0.002	14	1.0	1.3	0.18
41	1.7	13	0.8	3.4	10	< 0.001	18	3.8	1.4	0.15
478	1.8	3.5	3.0	2.5	1.3	2.4	4.6	0.24	1.2	0.13

5. Results on material characterization

As shown in the previous two sections, the characteristics of the $PbWO_4$ crystals measured in this study, such as transmittance, emission spectra, decay times and radiation resistance, vary considerably from sample to sample. Material characterization, including determination of trace element impurities, defects and structural analysis, can help to provide information on these various properties. In this investigation, an initial attempt has been made to identify possible deviations from stoichiometric $PbWO_4$ for sample 768, and to identify trace element impurities in a number of the other samples. All material characterization was performed by the independent analysis firm of Charles Evans and Associates [21].

A quantitative wavelength dispersive Electron Microprobe (EMPA) analysis was done on sample 768, and Particle Induced X-ray Emission (PIXE) analyses were performed on samples 767 and 768, to identify possible deviations from stoichiometric $PbWO_4$. The results showed that these crystals were essentially pure stoichiometric $PbWO_4$. However, there was an indication that the W/Pb ratio decreased by up to 5% from the small end to the large end in both crystals.

Glow Discharge Mass Spectroscopy (GDMS) was used to search for trace element impurities in all five large samples and three small samples: SIC 34, SIC 41 and Borogoditsk 478. A survey of 77 elements revealed impurities at the few ppm to sub-ppm level in all samples. Table 5 lists the impurities detected in a portion of each sample, taken 3 to 5 mm below the surface of the crystal, i.e. no surface contamination. All detected impurities at a level greater than 1 ppm are listed, in addition to the sum of the transition metals (TM): Sc, Ti, V, Cr, Mn, Fe, Co, Ni, Cu and Zn, and the sum of detected rare earth elements (RE): Ce, Pr, Nd, Eu, Sm, Gd, Tb, Dy, Ho, Er, Tm, Yb and Lu. The transition metals and rare earth elements were found to be adversely affect the radiation resistance of BGO and BaF_2, respectively [6].

From the GDMS analysis, the following observations can be made:

- All samples from Bogoroditsk have significant Nb and Mo, while samples from SIC have no detectable Nb.
- The trace element Mo seems to be related to the slow scintillation components, e.g. sample 478 and 728 have the lowest Mo content.
- There seems to be no obvious correlation between the detected trace element impurities and the susceptibility to radiation damage, indicating that defects, such as oxygen vacancies, may play an important role in determining the radiation hardness.

However, it should be noted that GDMS is essentially a bulk analysis technique which detects only those impurities which are contained a small sample. It is possible that higher concentrations of impurities are present in certain localized areas, or inclusions, in the crystals. This was, in fact, the case for BaF_2 [6]. Other analytical techniques, such as Secondary Ionization Mass Spectroscopy (SIMS), can be employed to better determine if such effects are present in $PbWO_4$ crystals.

6. Summary and discussion

6.1. Optical properties

The longitudinal transmission of full size $PbWO_4$ crystals from Bogoroditsk shows significant absorption below 500 nm, as shown in Fig. 5. However, since the scintillation emission is peaked at 500 nm, these crystals provide acceptable light attenuation lengths and light response uniformity. This explains the excellent energy resolution with a constant term of less than 0.5% obtained in CERN beam tests [1]. The blue absorption of full size crystals, however, may still present a serious problem, since it prevents the propagation of the blue light in the crystal. As discussed in Section 3.3, the blue light has a short decay time, and is thus more desirable for a fast calorimeter. In addition, there seems to be a correlation between the absorption at 370 nm and the radiation hardness of the crystal, as discussed in Section 4. It is thus important to understand its origin, and to eliminate the blue absorption in full size crystals.

All full size $PbWO_4$ crystals from Bogoroditsk have a radioluminescence which is peaked at 500 nm, and a 20 to 30 nm blue shift as compared to the photoluminescence, as

shown in Fig. 7. Measurements on small crystals from SIC and Bogoroditsk, however, show that some crystals have an emission peaked in the blue region, and they have smaller very slow components, as shown in Figs. 8 and 12. This observation agrees with previous results [18]. Our measurements also confirm an early observation that the emission of $PbWO_4$ crystals may be affected by different annealing processes in crystal growth [19]. The samples annealed in vacuum (SIC 34) and in an oxygen-rich atmosphere (SIC 41) indeed have different emission peaks. This indicates that the blue and the green luminescence centers in the $PbWO_4$ are possibly structure or oxygen content related. However, the change in absorption, i.e. the shift of the absorption edge to longer wavelengths, may also cause an apparent shift of the emission spectrum, if the intrinsic scintillation of $PbWO_4$ crystal contains both blue and green components.

The total light yield of full size $PbWO_4$ crystals, integrated in a 100 ns gate, is up to 10 p.e./MeV, as measured by a PMT with a bialkali photocathode (Hamamatsu R2059). It can be converted to $\sim$ 100 photons/MeV, assuming the emission weighted quantum efficiency is 10.4%, as shown in Fig. 9.

The decay time of the scintillation light from $PbWO_4$ can be parameterized by three components: one fast ($<$ 10 ns), one slow (20 to 200 ns), and one very slow (500 ns to a few μs), as shown in Figs. 11, 12 and 13. The fraction of the very slow component was observed to be larger for recently grown full size $PbWO_4$ crystals, although all have similar light yields measured with 50 and 100 ns gates. For crystals which have their main emission peak in the blue region (Bogoroditsk 478 and SIC 34), the fraction of the very slow component is significantly less than those with their emission peaked in the green region. Since the slow component is not useful for LHC applications, and the residual slow component from previous beam crossings could introduce additional readout noise, it is desirable to understand the origin of the slow component and to minimize it by optimizing the crystal growth process.

6.2. Radiation damage

As shown in Section 4, it appears that $PbWO_4$ crystals are intrinsically radiation hard, but currently produced production size $PbWO_4$ crystals suffer from radiation damage at different levels. The scintillation mechanism seems to be unaffected by irradiation with ^{60}Co γ-rays up to 1 Mrad, and the effect of radiation induced phosphorescence seems to not have serious consequences in situ at the LHC. The main consequence of radiation damage for $PbWO_4$ is the radiation induced absorption, or color center formation. This absorption causes a degradation of the transmittance and light attenuation length, and hence the detectable light output. It should be pointed out that the CMS $PbWO_4$ crystal calorimeter is more sensitive to the color center formation than what has been shown in this investigation. This is due to the fact that the average path length of light collected by a small area avalanche photodiode (APD) is longer than that by a PMT covering the entire back face of the crystal [23]. The APD readout thus is more sensitive to the change in light attenuation length caused by color center formation.

The five full size crystals can be divided into two groups: (1) samples 728 and 768, which show significant radiation induced absorption and significant degradation in light output, (2) samples 767, 1015 and 1022 which show much less damage. The radiation resistance seems to be correlated with the longitudinal transmittance at 370 nm. While crystals 728 and 768 have very low transmittance at 370 nm, crystals 767, 1015 and 1022 have a knee below 400 nm, and sample 767 has the highest transmittance at 370 nm.

The degradation of the transmittance, light attenuation length and the light output saturates after a few krad. This indicates that the radiation damage observed in $PbWO_4$ is related to intrinsic impurities or defects, and that the radiation does not create additional defects. For crystals with better radiation resistance, the reduced light output is about 50 to 80% of the initial value, which is still adequate for a precision calorimeter at LHC. However, the damage recovers at room temperature with a time constant of about 160 h, which would cause a serious problem with a time-dependent response in situ, and thus affect the stability of the calorimeter. This can be compared to performance of BaF_2 crystals, whose damage saturated at a few krad, but does not recover at room temperature [22].

It is also important to note that, although the change of transmittance or light attenuation length (and thus the light output) can be calibrated in situ by an appropriate light monitoring system, the change in light attenuation length, however, may destroy the light response uniformity. The consequence of a degraded light response uniformity is a degraded energy resolution which can not be corrected by the monitoring system [22]. It is thus important to reduce the magnitude of the saturated radiation damage in $PbWO_4$ by reducing damage related impurities and defects as much as possible.

Optical bleaching and thermal annealing were found to be effective in removing bleachable color centers in the crystal. Although thermal annealing is not practical in situ, optical bleaching, in principle, could be implemented by sharing the same optical fiber system used for light monitoring and calibration [24]. This was the solution for production BaF_2 crystals to be used to construct a precision calorimeter at the SSC [22]. However, the ultimate solution would be to improve the crystal quality to a level where the radiation damage is negligible. Optical bleaching in situ would then only be used as a last resort, if improvements in the crystal quality were no longer possible or cost effective.

6.3. Material characterization

The identification of impurities, defects and structural changes are crucial for $PbWO_4$ crystal development, since they are possibly responsible for the blue absorption, the

slow decay components and the susceptibility to radiation damage. Our analysis indicates that some impurities, such as Mo, may be responsible for the slow components. However, there seems to be no obvious correlation between the detected trace element impurities and the susceptibility to radiation damage, indicating an important role of defects, such as oxygen vacancies, in these processes, or that impurities may exist in inclusions.

Further analysis in this aspect is certainly an important part of the $PbWO_4$ development program. In developing radiation-hard BaF_2 crystals, various analytical techniques were used, including PIXE, EMPA, GDMS, Secondary Ionization Mass Spectroscopy (SIMS), Atomic Absorption Spectrum (AAS), Rutherford Back Scattering (RBS), Electron Spin Resonance (ESR), Electron-Nuclear Double Resonance (ENDOR), Neutron Activation Analysis (NAA), Transmission Electron Microscopy (TEM) and Scanning Electron Microscopy (SEM). It is important that all necessary characterization means be used to establish a correlation between the crystal performance and impurities and defects in the crystals.

7. Conclusions

Since the discovery of $PbWO_4$ as a scintillating crystal, much work has been devoted to (1) production of large, calorimeter-sized crystals, (2) understanding their performance and (3) improvements in crystal quality, especially radiation resistance. The investigation described in this report is an integrated part of this effort. At this time, production size crystals can be mass produced at Bogoroditsk and SIC, and the quality of these crystals approach what is required by the CMS collaboration at LHC. There are, however, existing problems in production size crystals, such as the blue absorption, the slow components and the time-dependent performance under irradiation. A rigorous R&D program, including crystal evaluation and material analysis, is necessary to understand the origin of these effects, and to reduce or eliminate these problems. It is expected that $PbWO_4$ crystals capable of providing a stable, precision electromagnetic calorimeter for CMS at the LHC will be developed as a result of this R&D program.

Acknowledgements

We would like to thank Dr. P. Lecoq for providing $PbWO_4$ samples grown in Bogoroditsk and Prof. Z.W. Yin for providing $PbWO_4$ samples grown at SIC. Many inspiring and interesting discussions with Drs. E. Auffray, B. Borgia, I. Dafinei, P. Denes, M. Kobayashi, M. Korzhik, P. Lecoq, M. Schneegans, J. Virdee and Z.W. Yin are also acknowledged.

References

[1] Compact Muon Solenoid Technical Proposal, CERN/LHCC 94-38, LHCC/P1 (1994).
[2] L* Letter of Intent to the SSC Laboratory, November 1990.
[3] GEM Letter of Intent, SSCL SR-1184, November 1991.
[4] Compact Muon Solenoid Letter of Intent, CERN/LHCC 92-3, LHCC/I1 (1992).
[5] L3P Letter of Intent, CERN/LHCC 92-5, LHCC/I3 (1992).
[6] G. Gratta, H. Newman and R.Y. Zhu, Annu. Rev. Nucl. Part. Sci. 44 (1994) 453.
[7] Crystal Clear Collaboration, see S. Anderson et al., Nucl. Instr. and Meth. A 332 (1993) 373.
[8] M. Kobayashi et al., Nucl. Instr. and Meth. A 333 (1993) 429.
[9] O. Buyanov et al., Nucl. Instr. and Meth. A 349 (1994) 62;
S. Inaba et al., Nucl. Instr. and Meth. A 359 (1995) 485;
G. Alexeev et al., Nucl. Instr. and Meth. A 364 (1995) 307.
[10] J.P. Peigneux, Nucl. Instr. and Meth. A 351 197 (1994).
[11] P. Lecoq et al., Nucl. Instr. and Meth. A 365 (1995) 291.
[12] See, for example, presentations given by M. Kobayashi et al., P. Lecoq et al. and C. Woody et al., in: Inorganic Scintillators and their Applications, eds. P. Dorenbos and C.W. van Eijk (Delft University Press, 1995).
[13] D.A. Ma and R.Y. Zhu, Nucl. Instr. and Meth. A 333 (1993) 422.
[14] G. Bakhshiva and A. Morozov, Sov. J. Opt. Technol. 44 (1977) 9.
[15] S. Baccaro et al., CMS TN/95-065, June 1995.
[16] P.W. Levy, J. Phys. Chem. Solids 52 (1991) 319.
[17] L.M. Bollinger and G.E. Thomas, Rev. Sci. Instr. 32 (1961) 44.
[18] M. Kobayashi et al., in: Inorganic Scintillators and their Applications, eds. P. Dorenbos and C.W. van Eijk (Delft University Press, 1995) p. 286.
[19] Z.W. Yin et al., in: Inorganic Scintillators and their Applications, eds. P. Dorenbos and C.W. van Eijk (Delft University Press, 1995) p. 490.
[20] D.A. Ma and R.Y. Zhu, Nucl. Instr. and Meth. A 332 (1993) 113.
[21] Charles Evans and Associates, 301 Chesapeake Drive, Redwood City, CA 94063, USA.
[22] R.Y. Zhu, Nucl. Instr. and Meth. A 340 (1994) 442.
[23] R.Y. Zhu, Ray-tracing for $PbWO_4$ crystals, talk given in CMS ECAL Meeting, August 9, 1995.
[24] D.A. Ma, R.Y. Zhu and H. Newman, Nucl. Instr. and Meth. A 356 (1995) 309.